Experimental demonstration of coherent beam combining over a 7 km propagation path

Thomas Weyrauch,[1,*] Mikhail A. Vorontsov,[1,3] Gary W. Carhart,[2] Leonid A. Beresnev,[2] Andrey P. Rostov,[3] Ernst E. Polnau,[1] and Jony Jiang Liu[2]

[1]*Intelligent Optics Laboratory, School of Engineering, University of Dayton, 300 College Park, Dayton, Ohio 45469–2951, USA*

[2]*Intelligent Optics Laboratory, Computational and Information Sciences Directorate, United States Army Research Laboratory, 2800 Powder Mill Road, Adelphi, Maryland 20783, USA*

[3]*Optonicus, 711 East Monument Avenue, Suite 101, Dayton, Ohio 45402, USA*

**Corresponding author: thomas.weyrauch@udayton.edu*

Received August 9, 2011; revised October 11, 2011; accepted October 12, 2011; posted October 13, 2011 (Doc. ID 152671); published November 15, 2011

We demonstrate coherent combining (phase locking) of seven laser beams emerging from an adaptive fiber-collimator array over a 7 km atmospheric propagation path using a target-in-the-loop (TIL) setting. Adaptive control of the piston and the tip and tilt wavefront phase at each fiber-collimator subaperture resulted in automatic focusing of the combined beam onto an unresolved retroreflector target (corner cube) with precompensation of quasi-static and atmospheric turbulence-induced phase aberrations. Both phase locking (piston) and tip–tilt control were performed by maximizing the target-return optical power using iterative stochastic parallel gradient descent (SPGD) techniques. The performance of TIL coherent beam combining and atmospheric mitigation was significantly increased by using an SPGD control variation that accounts for the round-trip propagation delay (delayed SPGD).

OCIS codes: 140.3298, 010.1285, 010.1080.

Coherent combining of laser beams that originate from a fiber-based multichannel master oscillator power amplifier (MOPA) laser system at a remotely located target after propagation through the atmosphere requires adaptive compensation of both random phase shifts introduced by the MOPA system and atmospheric turbulence-induced phase aberrations [1,2]. Coherent beam combining, also referred to as phase locking, has been demonstrated in several laboratory-based experiments (see, e.g., [3–7]) and over a 408 m long distance in an outdoor experiment with a cooperative target [8].

In this Letter, we report the results of the first (to our best knowledge) successful coherent beam combining and turbulence mitigation experiments over an extended-length atmospheric propagation path in a target-in-the-loop (TIL) setting with a noncooperative target using adaptive control of the piston (subaperture-averaged phase) and tip and tilt corrections at each fiber-array subaperture. The round-trip propagation delay issue—a major obstacle for TIL adaptive optics techniques—was overcome by utilizing the recently proposed "delayed" stochastic parallel gradient descent (SPGD) wavefront control technique [9], which allowed the duration between wavefront control updates to be shorter than the round-trip propagation delay and resulted in a significant increase of compensation bandwidths.

The setup used in the experiments (Fig. 1) consists of the following major subsystems: (i) a seven-channel master oscillator power amplifier (MOPA) system based on single-mode, polarization-maintaining (PM) fiber elements; (ii) a fiber-collimator array with built-in capabilities for electronic control of wavefront phase tip and tilts at each fiber-collimator subaperture; (iii) an unresolved target (a corner-cube retroreflector) located at 7 km distance; (iv) a receiver telescope for measurements of the target-return optical wave power, referred to as the power-in-the-bucket (PIB) metric, J; and (v) a control unit that includes piston (phase-locking) and tip–tilt phase control subsystems.

In the MOPA system, the light from a narrow-linewidth (~5 kHz) fiber laser with wavelength $\lambda = 1064$ nm and single-mode PM fiber output is divided into seven channels using a fiber splitter with integrated, electrically controlled phase-shifting elements from EOSPACE [10]. The MOPA system output fibers, each with a mode field diameter of 7 μm, are connected to a fiber-collimator array (Optonicus INFA 7C [11]). In the fiber array, the tip of each output fiber is placed in the focus of the corresponding collimating aspheric lens with a clear aperture diameter of $d = 33$ mm and a focal distance of $f = 174$ mm. The closest center-to-center distance between the collimating lenses in the array is 37 mm, and the entire fiber-array aperture is 107 mm. The output fibers are mounted inside special fiber-positioner devices with piezo-actuators that can independently displace the fiber tips within a $\pm 35\,\mu$m range in two lateral directions [11,12]. These fiber-tip displacements result in controllable deviations of the propagation directions of the outgoing beams anywhere within a ± 0.2 mrad solid angle about the optical axis and were used to provide precise overlapping of the outgoing beams at a remote target (electronic beam focusing) as well as precompensation of wavefront phase tip and tilt static and dynamic aberrations [4].

The outgoing beams with a combined optical power of 12 mW were transmitted through a window located in the Intelligent Optics Laboratory at the fifth floor of the University of Dayton's College Park Center building (15 m above ground) and propagated toward the corner-cube retroreflector (50 mm aperture) located in a shed on the rooftop of a 40 m high building 7 km away. The laboratory double-glass window introduced significant phase aberrations with a peak-to-valley (PV) amplitude of $\sim 1.0\lambda$ over the fiber-array aperture and $\sim \lambda/4$ PV over fiber-array subapertures. The impact of these quasi-static aberrations was partially mitigated using the adaptive tip–tilt control system.

The optical wave returning from the target entered a receiver telescope (aperture 20 cm) located near the fiber-array transmitter, as shown in Fig. 1(b). The received light was divided between a CCD camera and a photodiode for telescope pointing (target imaging) and the received light power measurements, respectively. The photodiode output signal was used as the performance metric, J, for both the phase locking and the tip–tilt control subsystems.

The two parallel operating control subsystems were both based on the maximization of the PIB metric, J, using an asynchronous SPGD control technique with significantly different (~48 times) iteration rates [13]. The tip–tilt control subsystem with 14 control channels (two per fiber collimator) utilized a personal computer with analog input/output cards and a set of high-voltage amplifiers (± 70 V) for generation of the control voltages $\{u_j^{(n)}\}$ $(j = 1, \ldots, 14)$, which were applied to the piezo-actuators. At each tip–tilt iteration, (n), a control voltage update was performed using the conventional SPGD algorithm [13]

$$u_j^{(n+1)} = u_j^{(n)} + \gamma \delta u_j^{(n)} [J_+^{(n)} - J_-^{(n)}], \qquad (1)$$

where γ is the gain coefficient and $\{\delta u_j^{(n)}\}$ is a set of 14 small-amplitude random control voltage changes, denoted as perturbations. The perturbations in the form $\{\delta u_j^{(n)}\}$ (positive) and $\{-\delta u_j^{(n)}\}$ (negative) are applied between two sequential updates of the control voltages. In Eq. (1), $J_+^{(n)}$ and $J_-^{(n)}$ are the measured PIB metric values that correspond to the positive and negative perturbations. The characteristic time τ_{SPGD} (SPGD cycle time) between sequential control voltage updates is given by

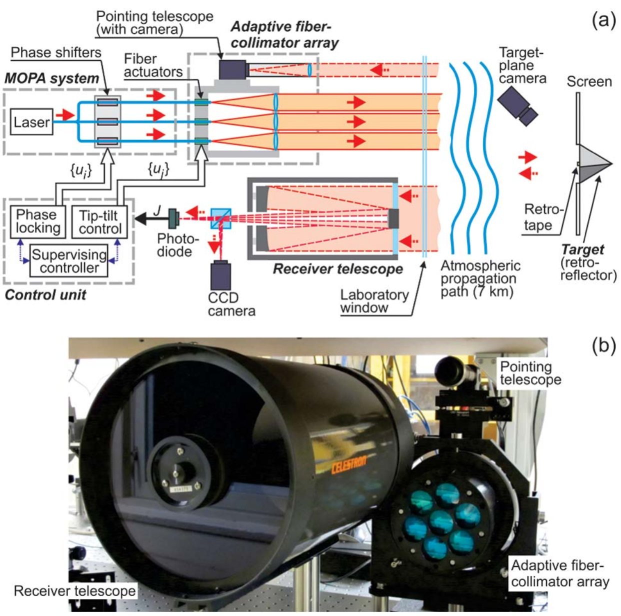

Fig. 1. (Color online) (a) Schematic of the experimental setup used for coherent beam combining over a 7 km atmospheric propagation path. (b) Photo of the fiber-array transmitter with the pointing telescope (right) and the receiver telescope (left).

$$\tau_{\mathrm{SPGD}} = 2(\tau_{\mathrm{pert}} + \tau_{\mathrm{resp}} + \tau_J + \tau_{\mathrm{delay}}), \qquad (2)$$

where τ_{pert} is the time required to perturb the control voltages, τ_{resp} is the delay between a control voltage change and the corresponding optical phase response, τ_J is the PIB metric measurement time, and τ_{delay} is the delay between an induced wavefront phase variation and the corresponding metric change. The last term in Eq. (2) is the double-pass delay $\tau_{\mathrm{delay}} = 2L/c$ caused by the optical wave propagation over the distance L with the speed of light, c (in the experimental setting $L = 7$ km and $\tau_{\mathrm{delay}} = 46.7\,\mu$s). The tip–tilt SPGD cycle time, τ_{SPGD} in Eq. (2), is mainly limited by the time response of the piezo-actuators, $\tau_{\mathrm{resp}} \approx 120\,\mu$s, which is significantly longer than τ_{delay} and $\tau_J \approx 20\,\mu$s. The resulting tip–tilt subsystem SPGD iteration rate $f_{\mathrm{SPGD}} = 1/\tau_{\mathrm{SPGD}}$ was $f_{\mathrm{SPGD}} \approx 3$ kHz.

The piston phase control subsystem utilized the fiber-integrated phase shifters of the MOPA system, which have a short response time of $\tau_{\mathrm{resp}} < 10$ ns so that the limiting factor for increasing the SPGD control iteration rate is the double-pass delay time τ_{delay}. Considering $\tau_{\mathrm{delay}} = 46.7\,\mu$s, the piston-phase control SPGD cycle time is at least ~100 μs and thus $f_{\mathrm{SPGD}} \leq 10$ kHz. Note that the SPGD + CU 8D controller from Optonicus used in the experiments can provide much higher iteration rates (up to ~250 kHz) [10]. Therefore, the propagation delay imposed the limit on the operational bandwidth of the conventional SPGD-based piston-phase control subsystem and its capability for mitigation of atmospheric turbulence-induced aberrations.

In order to overcome this problem, we utilized in the piston-phase control subsystem the recently proposed delayed-SPGD wavefront control algorithm, where the iterative procedure of the control voltage update during each iteration cycle (n) can be described by the following rule [9]:

$$u_i^{(n+1)} = u_i^{(n)} + \gamma [J_+^{(n)} - J_-^{(n)}] \delta u_i^{(n-\Delta n)}, \qquad (i = 1, \ldots, 7). \qquad (3)$$

Here the integer number $\Delta n > 0$ is the delay parameter that accounts for the double-pass propagation time. In Eq. (3), Δn links the variation of the metric $\delta J^{(n)} = [J_+^{(n)} - J_-^{(n)}]$ measured during iteration (n) to the control signal perturbations $\{\delta u_i^{(n-\Delta n)}\}$, which caused the metric change. The delay parameter can be calculated as the closest integer number to the ratio $\tau_{\mathrm{delay}}/\tau_{\mathrm{SPGD}}$. With the SPGD cycle time $\tau_{\mathrm{SPGD}} = 7.0\,\mu$sec (iteration rate $f_{\mathrm{SPGD}} \approx 143$ kHz) and $\tau_{\mathrm{delay}} = 46.7\,\mu$s, we obtain $\Delta n = 7$.

During the experiments, the fiber-collimator array control system was repeating 50 sequences of 5.25 s long trials comprising three operational states of 1.75 s each. These stages are indicated in Fig. 2 as “feedback off” (all control loops were off), “piston control on,” and “piston and tip–tilt control on.” In the “piston control on” state, the piston-phase (phase-locking) control system was turned on. During the last state, both the piston and tip–tilt control subsystems were switched on. Values for the PIB metric, J, were recorded for all 50 trials by the supervising controller at a rate of about 10 k samples/s.

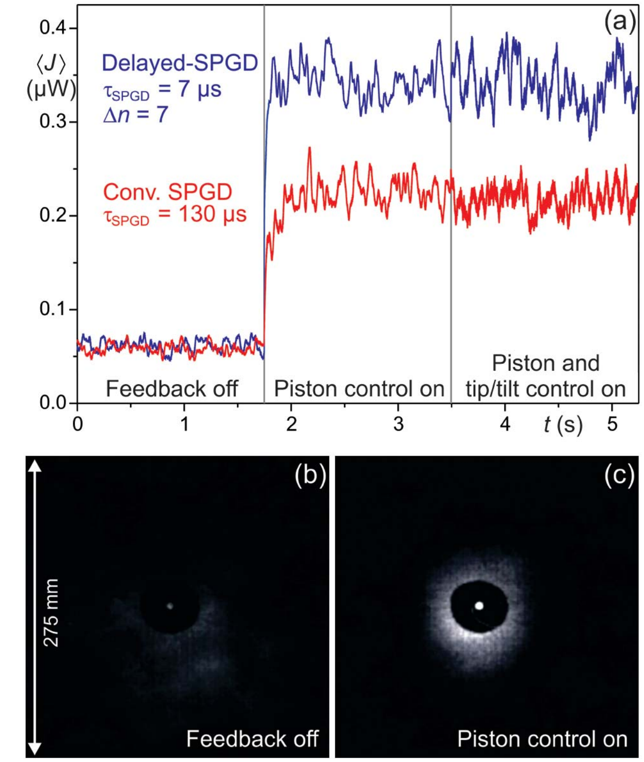

Fig. 2. (Color online) Experimental results from the coherent beam combining experiment: (a) average PIB metric evolution curve, $\langle J \rangle$ and (b), (c) averaged irradiance distribution at the target plane with feedback off (b) and piston control on (c).

As shown in Fig. 1(a), the retroreflector at the target plane was mounted behind a hole in a cardboard screen and a small piece of retroreflecting tape (~6 mm diameter) was glued onto the center of the retroreflector's cover glass. An near-IR camera with a wide-angle objective was placed about 1 m in front and 20 cm to the side of the retroreflector and used to image the irradiance pattern (beam footprint) on the screen and the retrotape.

Figure 2(a) shows the time dependence of the trial-averaged PIB metric $\langle J \rangle$ for two different settings of the piston-phase controller: the first curve (red, lower) corresponds to the conventional SPGD algorithm (1) and the second curve (blue, upper) to the delayed algorithm (3). In comparison to the open loop state, the average PIB metric, $\langle J \rangle$, increased 3.7-fold for the conventional and 5.6-fold for the delayed-SPGD control.

Recorded target-plane beam footprints (averages of 270 frames) for the cases with feedback off and piston-phase control on can be seen in Figs. 2(b) and 2(c), respectively. The dark annular region in the center corresponds to the circular opening for the retroreflector with the retrotape spot in the center. A comparison of these two images demonstrates the higher concentration of the beam energy at the retroreflector when phase control is on and proves that the PIB metric maximization locks the beam phases at the target plane.

The experimental results in Fig. 2(a) correspond to atmospheric turbulence conditions characterized by a path-averaged refractive index structure parameter $C_n^2 = 6 \times 10^{-16}\ \mathrm{m}^{-2/3}$ (measured by a Scintec BLS2000 scintillometer [14]) and a normalized standard deviation of metric fluctuations $\sigma_J/\langle J \rangle = 0.92$ (open loop). Piston control resulted not only in the increase of the average metric value, but also led to a decrease in the metric fluctuation level down to $\sigma_J/\langle J \rangle = 0.52$ for the conventional and to 0.42 for the delayed SPGD controllers.

Note that the tip–tilt control subsystem, which was turned on during the last state of the adaptation trials, did not result in a further metric increase (and caused only a slight change in metric fluctuations due to the tip–tilt perturbations). This can be explained by taking into account the 48-fold faster updates of the piston-phase control system, which can provide a partial mitigation of overall wavefront phase tip and tilt aberrations using a stepwise (piston) approximation prior to a reaction of the tip–tilt subsystem. However, our experiments showed that efficient coherent combining with piston-phase control was only possible if the transmitted beams overlap well at the target, which was achieved by turning on the tip–tilt control subsystem for a few seconds in addition to piston control. In the experiments described above, tip–tilt control voltages were fixed at the end of each adaptation trial and provided sufficient overlapping during the piston control stage of the next adaptation cycle. Without a tip–tilt control phase in each trial, we observed a slow (on the order of 100–200 s) decline in coherent beam combining efficiency, indicating that static tip–tilt control voltages do not maintain efficient overlapping of the outgoing beams at the target over a longer time period, mostly due to thermal expansion-induced system misalignments.

This work was performed in the frame of collaborative agreement W911NF-09-2-0040 between the United States Army Research Laboratory and the University of Dayton.

References

1. M. A. Vorontsov and S. L. Lachinova, J. Opt. Soc. Am. A **25**, 1949 (2008).
2. S. L. Lachinova and M. A. Vorontsov, J. Opt. Soc. Am. A **25**, 1960 (2008).
3. H. Bruesselbach, S. Wang, M. Minden, D. C. Jones, and M. Mangir, J. Opt. Soc. Am. B **22**, 347 (2005).
4. M. A. Vorontsov, T. Weyrauch, L. A. Beresnev, G. W. Carhart, L. Liu, and K. Aschenbach, IEEE J. Sel. Top. Quantum Electron. **15**, 269 (2009).
5. V. Jolivet, P. Bourdon, B. Bennaï, L. Lombard, D. Goular, E. Pourtal, G. Canat, Y. Jaouën, B. Moreau, and O. Vasseur, IEEE J. Sel. Top. Quantum Electron. **15**, 257 (2009).
6. X. L. Wang, Y. X. Ma, P. Zhou, H. T. Ma, X. Li, X. X. Xu, and Z. J. Liu, Laser Phys. **19**, 984 (2009).
7. B. Pulford, T. Shay, J. Baker, A. Flores, C. Robin, C. Vergien, C. Zeringue, D. Gallant, A. D. Sanchez, C. Lu, and A. Lucero, in *Conference on Lasers and Electro-Optics*, OSA Technical Digest (CD) (Optical Society of America, 2010), paper CThO5.
8. H. Bruesselbach, S. Wang, M. Minden, C. Jones, and M. Mangir, in *2005 Conference on Lasers & Electro-Optics* (IEEE, 2005), Vol. 1, pp. 746–748.
9. M. A. Vorontsov and G. W. Carhart, Invention disclosure ARL No. 12-03 (U.S. Army Research Laboratory, 2011).
10. www.eospace.com.
11. www.optonicus.com.
12. L. A. Beresnev and M. A. Vorontsov, Proc. SPIE **5895**, 58950R (2005).
13. M. A. Vorontsov and G. W. Carhart, J. Opt. Soc. Am. A **23**, 2613 (2006).
14. www.scintec.com.